Prototype Tracking Studies for Proton CT

Nate Blumenkrantz, Jason Feldt, Jason Heimann, Hartmut F.-W. Sadrozinski, *Senior Member, IEEE*, Abe Seiden, David C. Williams, Vladimir Bashkirov, Reinhard Schulte, Mara Bruzzi, David Menichelli, Monica Scaringella, G.A. Pablo Cirrone, Giacomo Cuttone, Nunzio Randazzo, Valeria Sipala, and Domenico Lo Presti

***Abstract*—As part of a program to investigate the feasibility of proton computed tomography, the most likely path (MLP) of protons inside an absorber was measured in a beam experiment using a silicon strip detector set-up with high position and angular resolution. The locations of 200 MeV protons were measured at three different absorber depth of PMMA (3.75, 6.25 and 12.5 cm) and binned in terms of the displacement and the exit angle measured behind the absorber. The observed position distributions were compared to theoretical predictions showing that the location of the protons can be predicted with an accuracy of better than 0.5 mm.**

***Index Terms*—Proton beams, Tomography, Silicon Radiation Detectors, Position Sensitive Particle Detectors**

I. Introduction

PROTON radiation therapy is one of the most precise forms of non-invasive image-guided cancer therapy. It is based on the well defined range of protons in material, with low entrance dose, a dose maximum ("Bragg peak") and a rapid distal dose fall-off, providing better sparing of healthy tissue and allowing higher tumor doses than conventional radiation therapy with photons. At present, the potentials of proton therapy cannot be fully exploited because the conversion of Hounsfield values, measured with x-ray computed tomography (CT), to relative electron density values is not always accurate [1]. The resulting uncertainties can lead to range errors from several millimeters up to more than 1 cm depending on the anatomical region treated. Additional uncertainties exist with respect to the target position relative to normal tissues in the treatment room that could be minimized by using proton CT for guiding the therapy.

Manuscript received May 16, 2006. This work was supported in part by Calspace and the INFN 5th commission MOPI project.

J. Feldt, J. Heimann, N. Blumenkrantz, H. F.-W. Sadrozinski, A. Seiden and D. C. Williams are with SCIPP, UC Santa Cruz, CA 95064 USA (telephone: 831-459-4670, e-mail: hartmut @scipp.ucsc.edu).

V. Bashkirov and R. Schulte, are with Loma Linda University Medical Center, CA 92354 USA (e-mail: rschulte@dominion.llumc.edu).

M. Bruzzi, D. Menichelli, M. M.Scaringella are with INFN and Università di Firenze, Dipartimento di Energetica, Via S. Marta 3, 50139 Firenze, Italy, (telephone: +390554796449, e-mail: bruzzim @fi.infn.it).

G.A. P. Cirrone, G. Cuttone are with INFN Laboratori Nazionali del Sud, Via S. Sofia, Catania Italy (e-mail: cirrone@lns.infn.it).

N. Randazzo, V. Sipala, D. Lo Presti are with INFN Sezione di Catania, 64, Via S. Sofia, I-95123 Catania, Italy . V. Sipala and D. Lo Presti are also with Department of Physics, University of Catania, 64, Via S. Sofia, I-95123 Catania, Italy (e-mail: nunzio.randazzo@ct.infn.it).

The long-term goal of our project is to develop the capability to use proton CT (pCT) instead of x-ray CT to minimize these uncertainties. We plan to test the hypothesis that a proton CT system based on single-particle tracking can provide electron density maps for proton treatment planning and dose verification that are more accurate and at least as dose-efficient as electron density maps obtained with kV x-ray CT. In particular, we hypothesize that the range uncertainty of protons in the brain can be minimized from the current value of 3-10 mm, to 1-3 mm.

Previous work reviewed in [2] and our own preliminary studies [3-9] indicate that proton CT based on tracking of individual protons traversing an object from many different directions and measuring their energy loss and scattering angle may yield accurate reconstructions of electron density maps with good density and spatial resolution, despite the fundamental limitation of Multiple Coulomb Scattering (MCS).

TABLE I
COMPARISON BETWEEN X-RAY CT AND PROTON CT

	X-ray CT	**Proton CT**	**pCT Challenge**
Measurement Principle	X-ray Absorption	Proton Energy Loss	Good Energy Resolution
Ensemble	Statistical	Individual Protons	High Speed DAQ
Trajectories	Straight line	Curved due to Multiple Coulomb Scattering (MCS)	High Resolution Tracking Find MLP
Reconstruction	Filtered Back Projection	Layer-by-Layer de-convolution	Curved Trajectories

II. PCT: Measurement principle and limitations

The requirement to measure single protons leads to the following conceptual design of the pCT scanner [8]: the proton locations and directions at the entrance and exit of the phantom/patient are measured each with a telescope consisting of two x-y planes of silicon detectors. The energy is measured in a hodoscopic array of calorimeter crystals. Details are given in Ref. [8].

The challenge of proton-by-proton pCT can be evaluated by

a comparison with its established alternative, x-ray CT. This is shown in Table I. We have encouraging results in essentially all critical challenges shown in Table I. While x-ray CT uses a statistical evaluation of the absorption via the Photoelectric and Compton effects, pCT measures the energy loss of individual protons. In previous studies we showed high contrast imaging using 140 MeV protons [3]. The dose is proportional to the square of energy resolution, thus mandating good energy determination. In addition to the energy resolution of the calorimeter, the energy resolution is limited by the natural energy straggling, which in 20 cm water is about 1-2%. Thus good energy resolution of better than 1% in the energy range from 100 to 200 MeV is required, and our results indicate that it can be achieved with crystals like CsI [9]. A detection of individual protons requires a data acquisition system capable of recording particle rates in excess of 1 MHz. We have developed such a system for the readout of silicon strip detectors [10]. The curved trajectories of the protons inside the phantom create difficulties for the image reconstruction as well, and instead of a straightforward Filtered Back Projection (FBP) algorithm, a layer-by-layer de-convolution has been employed [11], [12].

In contrast to x-rays, which either transverse the phantom unchanged or are absorbed, allowing the reconstruction algorithm to deal with straight lines between the source and the detector, protons are undergoing MCS, which changes the direction depending on the amount of material traversed and the energy. This behavior is well understood [13] and allows reconstructing the most likely path (MLP) inside the absorber when the entrance and exit trajectories are measured external to the absorber. An analytical calculation of the MLP as a function of material, depth, displacement and scattering angle has been derived in [6] but needs to be verified experimentally.

Thus all challenges in the last column of Table I have been met with the exception of the experimental verification of the theoretical MLP prediction in the absorber (phantom, patient), which is the objective of our beam experiment, described in detail below.

III. Most Likely Path

The theoretical MLP prediction (MLP) and associated one sigma and 2-sigma envelopes [6] use the well established Gaussian approximation of multiple scattering theory [13]. Fig. 1 shows predicted trajectories, indicating that the MLP depends strongly both on displacement and exit angle. One can see that for typical MLPs the expected uncertainty is of the order of 300 μm. The objective of the tracking studies presented here was to verify the theoretical predictions by tracking individual protons inside a segmented absorber.

IV. Beam Experiment Results: Tracking the Most Likely Path

A beam experiment with 200MeV protons was performed at the Loma Linda University Medical Center (LLUMC) synchrotron. The protons of 200 MeV energy were tracked with silicon strip detectors (SSDs) used before in the 1997 GLAST beam test [14].

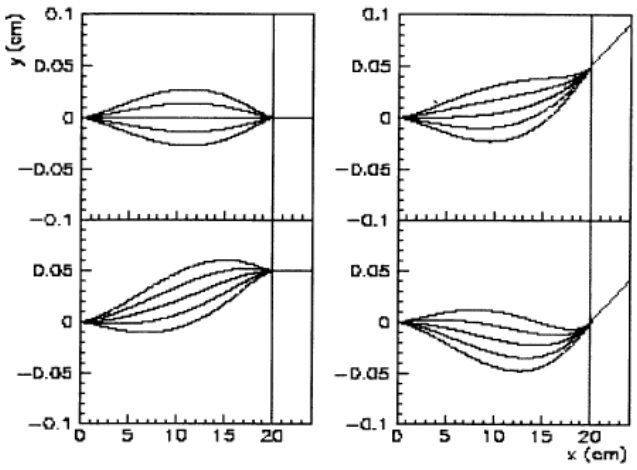

Fig. 1. Representative examples of MLPs including one- and 2-sigma envelopes of 200 MeV protons inside 20 cm of water [6]. These curves are colloquially called “bananas”.

In addition, a CsI calorimeter crystal provided energy measurement and a trigger for readout of the Si detector system.

A. Experimental Set-Up

Details of the experimental set-up and the data analysis are given in Ref [15], [16] and [17]. The set-up consisted of x-y silicon modules used as entrance and exit telescopes, and a CsI calorimeter (Fig. 2). The distance between the Si planes and the calorimeter was fixed during the runs. The set-up was flexible in that it allowed for insertion of 10 absorber plates (1.25 cm PMMA each) and a roving module between the telescopes. The following basic configurations were used: a) beam diagnostics, with two x-y planes both in entrance and exit telescopes, no absorber, b) MLP determination, with one entrance x-y plane and a roving plane between entrance and two exit Si planes. In the latter configuration, data were taken both without absorber (to check the dispersion), and with absorber to map out the MLP at different depths within the PMMA stack with the roving module.

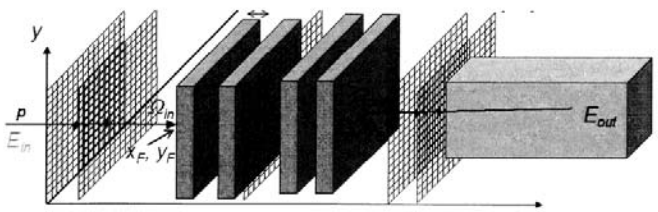

Fig. 2. Experimental layout: the 200MeV proton beam enters from left, is analyzed in the entrance telescope, passes through the segmented absorber (12 pieces of PMMA of 1.25 cm thickness each), and is again analyzed in the exit telescope before being stopped in the crystal. For beam diagnostic tests, the PMMA is removed and for MLP determination, one of the entrance telescope planes is employed as a roving module.

For runs with absorber in place, the first entrance module was removed and inserted at various depths within the PMMA stack to act as the roving module. The three different locations of the roving module at 3.75 cm, 6.25 cm and 12.5 cm depth of PMMA, are shown in Fig. 3. The beam diagnostic configuration allowed measuring the entrance location and angle of the protons, i.e. the beam size and beam spread, while the MLP determination set-up measured only the entrance location and not the entrance angle of the proton. Since the MCS angle turned out to be much larger than the beam spread, this was an acceptable solution.

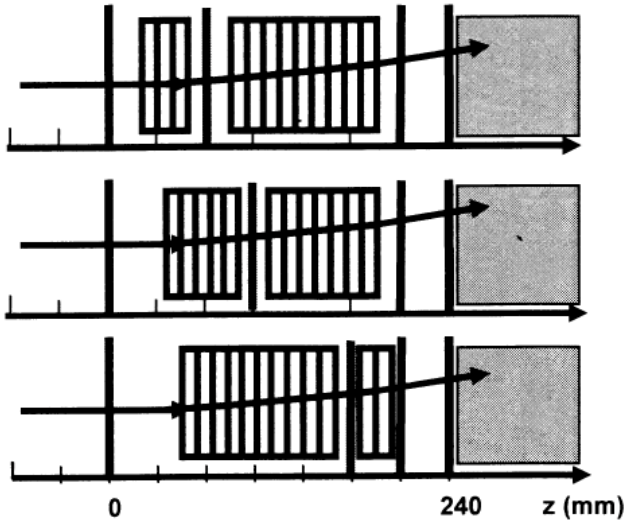

Fig. 3. Sketch of the three locations of the roving silicon module within the absorber stack (3.75 cm, 6.25 cm and 12.5 cm of PMMA, corresponding to z coordinates 5, 7.5 and 14cm, where the front of the PMMA is at the origin).

B. Beam Characteristics

We measured the characteristics of the 200 MeV proton beam and found a correlation between angle and position in both the horizontal and vertical directions, indicating a focus at about 5 m upstream. The beam divergence was of the order of 5 mrad. This beam spread is much smaller than the expected MCS angle of about 50 mrad, within the stack of PMMA plates, so that there was no need to measure the entrance angle for mapping out the MLP. Instead, a dispersion correction based on the measured entrance position was applied in lieu of the entrance angle measurement. Since the silicon strips provided a position resolution of the order of 80 μm and therefore a good angular resolution (of the order of 3mrad) we expect that the beam divergence and the MCS in the SSDs pose the practical limits of our experimental resolution.

C. Test of Multiple Coulomb Scattering Characteristics

The coordinates of the individual protons were transformed such that their entrance position and (inferred) direction was along the z-axis. Thus the x-y locations in the roving module and the exit telescope were expressed as the displacements relative to the initial proton direction, against which the exit angle was measured. The spread of the displacements at the three different locations of the roving module Y^{RMS}_{MCS} depends on the amount of absorber traversed and can be predicted by the Gaussian approximation of the MCS theory [13]. In addition the spread in the initial beam direction mentioned above caused an additional spread in displacements, Y^{RMS}_{beam}, which was determined by taking data without absorber. We expect that the observed Y^{RMS}_{ob} is the square root of the quadratic sum of these two contributions. In Table II we show the spread in the displacements as a function of the absorber depth. We find good agreement within 10-20%, indicating that the experimental spread is sufficiently explained by the beam characteristics and MCS. Thus, the intrinsic resolution of the instrument did not contribute significantly to the spread.

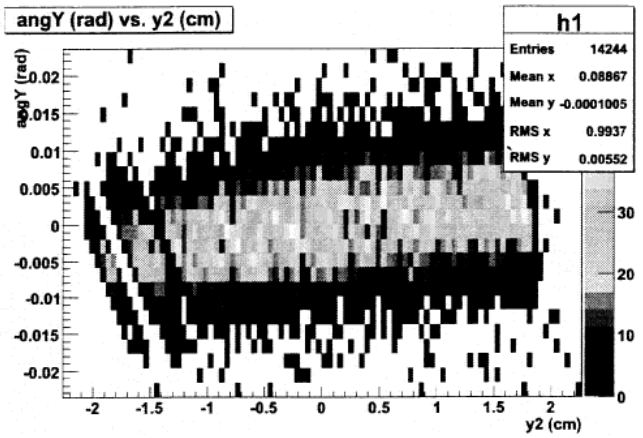

Fig. 4. Horizontal entrance angle vs. horizontal entrance position of the protons. The beam spread is about 5 mrad. There is a clear dispersion, which can be explained with a "fuzzy" focal plane at an upstream distance of about 5 m.

TABLE II
MEASURED AND PREDICTED SPREAD OF THE LATERAL DISPLACEMENTS IN THE ROVING MODULES AT DIFFERENT ABSORBER DEPTHS

Roving Location [cm]	No absorber Y^{RMS}_{Beam} [μm]	Absorb. (PMMA) depth [cm]	MCS Y^{RMS}_{MCS} [μm]	Expectation $\sqrt{(Y^{RMS}_{MCS})^2 + (Y^{RMS}_{Beam})^2}$ [μm]	Data Y^{RMS}_{ob} [μm]
5	320	3.75	334	460	550
7.5	460	6.25	693	830	920
14	760	12.5	2230	2350	2190

D. Correlation between exit displacement and exit angle

With the absorber present, the exit displacement with respect to the entrance position and the exit angle are highly correlated because individual scattering events determine both the exit angle and the lateral displacement. Fig. 5 shows this correlation. In addition, the need for fiducial cuts on displacement and exit angle is evident. Cutting events with displacement values larger than 4.5 mm and exit angle values larger than 55 mrad (as indicated in Fig. 5) reduces the number of events by 19%, but eliminates many events with either large scattering angle or with faulty measurement.

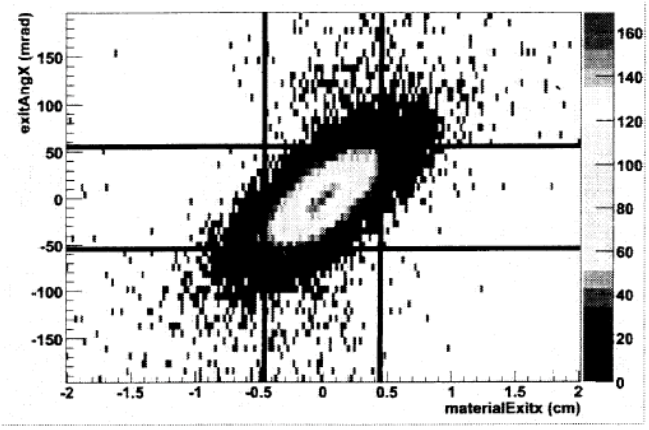

Fig. 5. Horizontal exit angle vs. horizontal exit displacement of the protons. The correlation between exit displacement and the exit angle due to multiple scattering is clearly seen. A cut on large displacements and large exit angles along the lines shown reduces the number of events from 33610 to 27201, i.e. by 19%.

E. Most Likely Path as a function of exit displacement and exit angle

The MLP analysis then correlates the displacement in the roving module (i.e. position relative to the entrance position) with the exit displacement and angle. From Fig. 1 one expects a positive correlation between the lateral displacement in the roving module and the displacement, and a negative correlation between the position in the roving module and the exit angle.

The displacements in the roving module are determined for bins of ± 200 μm in displacement at the material exit and ± 5 mrad in exit angle, respectively. This is shown in Fig. 6, where the displacement in the roving module at 5 cm depth is shown as a function of exit displacement for an exit angle of 30 mrad, and as a function of exit angle for a displacement of 0.3 cm. The expected correlations are indeed observed.

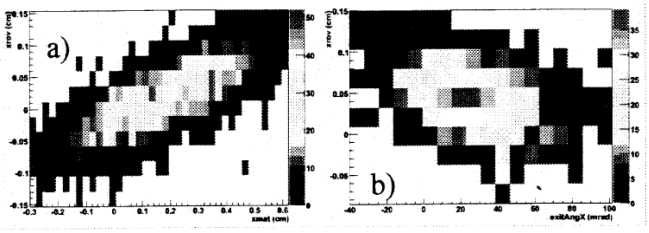

Fig. 6. Correlation between the displacement observed in the roving plane (vertical scale) and exit parameters on the horizontal scale: a) the displacement at the end of the absorber for fixed exit angle of 30 mrad and b) the exit angle for a fixed displacements of 0.3 cm.

For comparison between the measured displacements and the theory the original MLP predictions for uniform medium was modified to include the air gaps of about 1.5 cm in our set-up allowing for insertion of the silicon detectors. Fig. 7 shows the displacements in the roving modules located at different depths within the absorber for a few selected exit displacements and the prediction of the MLP calculated for the means in displacement and angle.

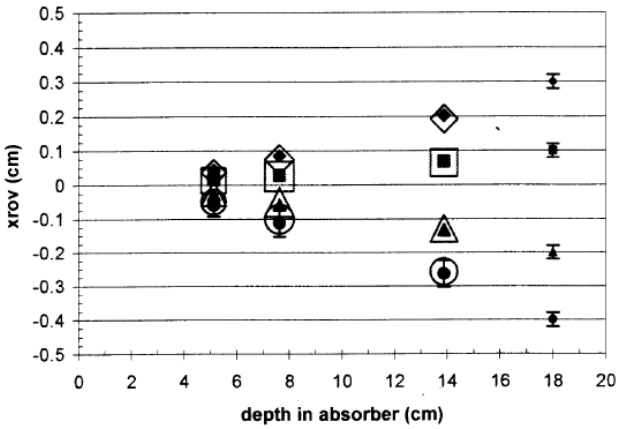

Fig. 7. Comparison of the displacement measured in the roving plane at different absorber depths for 4 different exit displacements (shown at 18 cm depth) with the analytical calculation of the most likely path MLP (open symbols: the size of the symbol is close to the MLP spread). The absorber depth includes the ~1.5 cm free space in front of the roving plane. The external parameters used are: exit displacement bins of ± 200 μm and exit angles from -80 mrad to +80 mrad. At 7.5 cm depth, the MLP predicts a one sigma band of 330 μm, while the measurement has an RMS = 480 μm.

The experimental data for an exit displacement of -0.4 cm are shown with their RMS variations, and the approximate spread in the theoretical prediction is indicated by the size of the symbols used. The prediction of the MLP is verified by the data within less than 200 μm, much less than the experimental spreads. This can only be a first step and has to be followed up by a procedure where the MLP is calculated for every proton and then averaged over, and a Monte Carlo study, that includes all instrument and beam effects.

F. Spreads in the Displacement Distributions within the Absorber

There are three different effects that can influence the spread in the roving modules. As mentioned before, the finite beam spread influences the spread of the experimental distributions. This has to be simulated with a full Monte Carlo program. Another is the bin size of the exit displacement selected. The third is introduced when defining the exit angle.

TABLE III
Measured Spread in the Roving Modules [μm]

z [cm]	Exp No angle correction	Exp with angle correction	Theor. MLP
5	370	340	250
7.5	480	410	330
14	450	400	280

Both the experimental spreads and the expected MLP spread are constant at a constant roving location for all displacements at the absorber exit. The spreads in the roving modules are shown in Table III. For comparison, the spreads

of the MLP are shown.

A marked reduction of the spread of the displacement in the roving module was observed when the information provided by the exit angle was used. This effect can be quantified by the slope of the correlation of roving displacement and exit angle Fig. 6b. The slopes are different for different roving position, depend only slightly on the exit displacement and are found to be identical for positive and negative displacements, as expected.

TABLE IV
SLOPE OF ROVING POSITION VS. EXIT ANGLE

z [cm]	Slope [cm/mrad]
5	$-6.5 \cdot 10^{-4}$
7.5	$-8.5 \cdot 10^{-4}$
14	$-9.5 \cdot 10^{-4}$

Since the exit angle spans range of about 50 mrad for every displacement (cf. the high intensity region in Fig. 5), the use of the exit angle in determining the roving position can result in a correction of about 300 to 500 μm, depending on the PMMA depth. Dividing the data into bins in angle reduces the experimental RMS of the roving displacements as shown in Table III.

TABLE V
DIFFERENCE BETWEEN EXPERIMENTAL ROVING DISPLACEMENTS AND MLP [μm]

	(z = 5 cm) Exit Displacement [cm]								
Exit angle [mrad]	-0.4	-0.3	-0.2	-0.1	0	0.1	0.2	0.3	0.4
-50	-86	-77	-59	-51					
-30	-87	-73	-58	-34	-19	-4			
0		-54	-28	-13	2	17	33	58	
30				10	24	37	61	75	88
50						-2	27	66	96

	(z = 7.5 cm) Exit Displacement [cm]								
Exit angle [mrad]	-0.4	-0.3	-0.2	-0.1	0	0.1	0.2	0.3	0.4
-50	-175	-172	-180	-188					
-30	-108	-102	-105	-99	-102	-106			
0		-19	-15	-1	2	6	19	23	
30				131	128	125	131	128	134
50						183	171	160	158

	(z = 14 cm) Exit Displacement [cm]								
Exit angle [mrad]	-0.4	-0.3	-0.2	-0.1	0	0.1	0.2	0.3	0.4
-50	-248	-282	-315	-349					
-30	-137	-147	-158	-169	-180	-181			
0		76	53	30	7	-16	-39	-62	
30				303	273	232	191	151	110
50						331	295	258	222

G. *Agreement between data and the MLP calculation*

The agreement between the data and the MLP calculation (modified for the finite air gaps at the position of the roving modules) has been tested for several exit displacements and angles. It was confined to values in these two parameters which contain about 80% of the data (see Fig. 5). The data were binned into bins of ± 200 μm in displacement at the material exit and ± 5 mrad in exit angle. The difference between the experimental displacement and the MLP prediction are shown in Table V for the three different positions of the roving module. There is agreement within about 350 μm, with growing disagreement at larger exit angles.

The effect the measurement of the angle has is shown in Fig. 8 for an exit displacement of 0.2 cm. The measured roving displacements are shown for three angles (0, 30, 50 mrad) and compared to the predicted MLP displacements. Measuring the angle corrects the data by several hundred microns, as expected from Table III. But at larger angles, the difference between the measurements and the MLP prediction increases. Thus the banana looks much more skinny in the experiment than in the MLP calculation. While experimental effects can't be excluded, since the alignment was verified to only one strip width of 236 μm and the beam divergence was not corrected for, we have started a comprehensive Monte Carlo (MC) study of the experiment and a comparison between the MLP calculation and the complete MC results including the beam characteristics and the resolution of the detectors [18]. This might lead to systematic corrections of the order a few 100 μm to the MLP prediction.

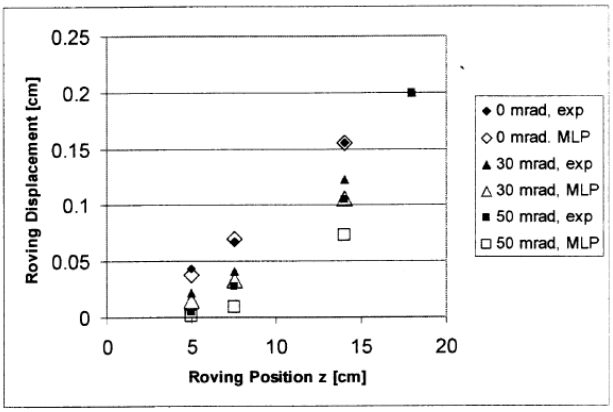

Fig. 8. Measured displacement in the roving modules at three different absorber depth for an exit displacement of 2 mm, for three different exit angle bins of equal bin size of ± 5mrad centered at an exit angle of 0.0, 0.03 and 0.05 (-1 exit angle σ). The absorber depth include the ~1.5 cm free space at the roving module.

The beam test proves that already at this stage, the location of the proton within the phantom/patient can be predicted to better than 0.5 mm, validating the MLP approach which uses only **external** track information for the prediction of the trajectories **inside** the phantom/patient.

V. FUTURE PLANS

The next steps are a beam test with an in-homogenous absorber (i.e. holes and inclusions at certain depths), followed by CT studies using a rotating phantom. This will require the use of both the tracker (measuring both positions and angles at

both entrance and exit) and the calorimeter, exploiting the full power of the pCT scanner.

VI. Conclusions

We have measured the most likely path of 200 MeV protons inside a segmented absorber of PMMA. The displacements of the protons from their original path agree well with the theory of multiple Coulomb scattering (MCS). We show that as expected from the theory of the most likely path (MLP) [6], we can predict the trajectory of the proton inside the absorber to better than 0.5 mm. This number is expected to improve when the effect of the beam divergence is eliminated with a measurement of the entrance angle of the proton.

Acknowledgment

We appreciate the smooth running of the LLUMC synchrotron.

References

[1] B. Schaffner and E. Pedroni, “The precision of proton range calculations in proton radiotherapy treatment planning: experimental verification of the relation between CT-HU and proton stopping power”, *Phys Med Biol*. 43(6):1579-1592, 1998.

[2] H. F.-W. Sadrozinski, V. Bashkirov, B. Keeney, L. R. Johnson, S. G. Peggs, G. Ross, T. Satogata, R. W. M. Schulte, A. Seiden, K. Shanazi, and D. C. Williams, “Toward proton computed tomography”, *IEEE Trans. Nucl. Sci*, vol 51, no.1, pp. 3-10, Feb. 2004.

[3] L. R. Johnson, B. Keeney, G. Ross, H. F.-W. Sadrozinski, V. Bashkirov, R. W. Schulte, K. Shahnazi. “Initial studies on proton computed tomography using a silicon strip detector telescope”, *Nucl Instr Meth* **A** 514 (2003) 215.

[4] HF-W Sadrozinski, M. Bruzzi, L.R. Johnson, B. Keeney, G. Ross, A. Seiden, D. C. Williams, L. Zhang, V. Bashkirov, R. W. Schulte, K. Shahnazi. “Issues in proton computed tomography”, *Nucl Instr Meth* **A** 511: (2003) 275-281.

[5] L. R. Johnson, B. Keeney, G. Ross, H. F.-W. Sadrozinski, A. Seiden, D. C. Williams, L. Zhang,V. Bashkirov, R. W. Schulte, K. Shahnazi, “Monte Carlo studies on proton computed tomography using a silicon strip detector telescope”. SCIPP 02/35.

[6] D C Williams, “The most likely path of an energetic charged particle through a uniform medium”, *Phys. Med. Biol*. 49 2899-2911, 2004.

[7] R. W. Schulte, V. Bashkirov, M. C. Klock, T. Li, A. J. Wroe, I. Evseev, D. C. Williams, T. Satogata, “Density resolution of proton computed tomography”, *Med Phys. 2005, 32:1035-46*

[8] R. W. Schulte, V. Bashkirov, T. Li, Z. Liang, K. Mueller, J. Heimann, L. R. Johnson, B. Keeney, H. F.-W. Sadrozinski, A. Seiden, D. C. Williams, L. Zhang, Z. Li, S. Peggs, T. Saratoga, C, Woody, “Conceptual design of a proton computed tomography system for applications in proton radiation therapy”, *IEEE Trans. Nucl. Sci., vol 51, no.3, pp 866 – 875, June 2004.*

[9] M. C. Klock, R. W. Schulte, V.Bashkirov, “First experimental calorimeter studies for proton CT at LLUMC”, *unpublished.*

[10] H. F.-W. Sadrozinski, V. Bashkirov, M. Bruzzi, M. Ebrahimi, J. Feldt, J. Heimann, B. Keeney, F. Martinez-McKinney, D. Menichelli, G.Nelson, G. Nesom, R. W. M. Schulte, A. Seiden, E. Spencer, J. Wray, and L. Zhang, “The particle tracking silicon microscope PTSM”, *IEEE Trans. Nucl. Sci., vol* 51, no.5, pp 2032 – 2037, Oct 2004.

[11] T. Li, Z. Liang, et al. “ Reconstruction with most likely trajectory for proton computed tomography”, *SPIE Medical Imaging*, 2004.

[12] T Li, Z. Liang, K. Mueller, J. Heimann, L. Johnson, H. F.-W. Sadrozinski, A. Seiden, D. Williams, L. Zhang, S. Peggs, T. Satogata, V. Bashkirov, and R. W. Schulte, “Reconstruction for proton computed tomography: a Monte Carlo study”, *IEEE NSS/MIC Conf Record* 2003

[13] Particle Data Group, S. Eidelman et al., “Review of Particle Physics”, *Physics Letters* B 592, 1 (2004).

[14] W. B. Atwood, S. Ritz, P.Anthony, R.P.Johnson, W.Kroeger, H.F.-W.Sadrozinski et *al.*, “Beam test of Gamma-ray Large Area Space Telescope components”, *Nucl.Instrum.Meth*. A446 (2000) 444-460.

[15] J. Heimann, “Developing an FPGA-based Readout for the pCT Detector System“, Senior Thesis, UC Santa Cruz Physics Dept., June 2005

[16] J. Feldt, “Preliminary Tracking Studies for Proton CT”, Masters Thesis, UC Santa Cruz Physics Dept., December 2005

[17] N. Blumenkrantz, “Tracking Study of 200 MeV Protons within a PMMA Phantom”, Senior Thesis, UC Santa Cruz Physics Dept., March 2006

[18] G. A. P. Cirrone et *al*, “Detailed Monte Carlo Investigation of a Proton Computed Tomography System”, Poster J03-25, 2005 IEEE NSS-MIC Symposium in Puerto Rico, Oct 2005.